A heuristic approach to output-only system identification under transient excitation

Hernán Garrido [a,b], Oscar Curadelli [a,b,1,*], Daniel Ambrosini [a,b]

[a] National University of Cuyo, Engineering Faculty, Mendoza, Argentina
[b] CONICET, National Research Council, Argentina

ARTICLE INFO

ABSTRACT

Output-only system identification is a very attractive technique for its implementation simplicity. However, it requires long records to validate the white-noise assumption of the excitation, mainly under transient forced vibration. Alternatively, free-vibration record segments can be selected before the identification process. This improves the accuracy, even using less data, but it requires human intervention or input recording. In the present paper, an approach is proposed for accurate system identification from short output-only records of vibration induced by transient excitation, without human intervention. The approach is based on a novel heuristic search algorithm to find free-vibration record segments, which is fully automatic and it handles the possibility of free-vibration absence. Tests with real-life data from Structural Health Monitoring (SHM) of a bridge showed that the free-vibration finding improves the accuracy of the modal parameter estimates up to ten times, as compared to using record segments starting at the response peak. The proposed approach drastically reduces the need to transmit large amounts of data, which impacts on hardware requirements of SHM implementations.

© 2016 Elsevier Ltd. All rights reserved.

1. Introduction

Many civil structures continue to be used regardless of ageing, damage accumulation and unknown risk of collapse (Salem & Helmy, 2014). Therefore, the ability to monitor their structural health is becoming increasingly important (Collins, Mullins, Lewis, & Winters, 2014; Dong, Song, & Liu, 2010; Farrar, Doebling, & Nix, 2001; Ko & Ni, 2005; Wong, 2004). Among the many strategies available within the Structural Health Monitoring (SHM) literature (Dong et al., 2010; Ko & Ni, 2005; Miguel, Miguel, Kaminski, & Riera, 2012; Wong, 2004), vibration-based methods are very attractive because of their simple hardware implementation and in-operation possibilities (Kramer, Smet, & Peeters, 1999). These methods consist in exciting the structural system and, through vibration measurements, identifying modal parameters that are correlated with its effective stiffness and strength (Chen & Zang, 2011; Ko & Ni, 2005; Miguel et al., 2012). Since artificial excitation has important practical limitations mainly in civil structures (Kramer et al., 1999), ambient- and operational-excitation sources are com-

monly exploited through the *output-only* approach (Peeters, 2000), in which the input is unknown. Today, many SHM programs implemented on structures around the world include this technique (Dong et al., 2010; Ko & Ni, 2005; Wong, 2004).

In general, all of the output-only system identification methods, such as Random Decrement Technique (Ibrahim, 1977), Peak Picking and refinements such as coherence function (Peeters, 2000), Ibrahim Time Domain (Ewins, 1984), and Stochastic Subspace Methods (Peeters, 2000), necessarily make the assumption that the excitation is white-noise. A recent and strong method to identify nonlinear models characterized by some form of nonlinear viscous dissipation forces and nonlinear restoring forces is proposed by Cavaleri and Papia (2014). However, as in previous cases, the hypothesis of white-noise excitation also was assumed. In the cases in which the input contains some dominant frequency components (colored-power-spectral-density function of excitation), it is difficult to separate them from the natural frequencies of the system (Peeters, 2000) leading to significant estimation errors. These problems may also appear when the non-stationary excitation is composed of *transient* impulses, indeed, if the impulsive load is of the *short-duration* type (Clough & Penzien, 1995), in which the response peak occurs during the free-vibration phase, a conservative start limit for a free-vibration record segment is obtained from the response peak; however, more sophisticated tools are needed in general cases where *repeated short- or long-duration* impulses can

* Corresponding author.
E-mail addresses: carloshernangarrido@yahoo.com.ar (H. Garrido), ocuradelli@fing.uncu.edu.ar (O. Curadelli), dambrosini@uncu.edu.ar (D. Ambrosini).
[1] Postal address: Facultad de Ingeniería. Centro Universitario, Parque Gral. San Martín, (5500) Mendoza, Argentina.

excite the system, in which the response peak occurs during the application of excitation, e.g. traffic loading on short-span bridges and gust loads on long-span bridges. As in others, output-only system identification methods have two additional problems associated with the excitation which may lead to significant estimation errors (especially in short-span bridges Farrar, Cornwell, Doebling, & Prime, 2000): (1) system mass variability, e.g. effect of heavy trucks (Kim, Jung, Kim, & Yoon, 1999); and (2) interaction with the structure, e.g. resonance of vehicle suspensions due to unevenness of the road (De Roeck, Maeck, Michielsen, & Seynaeve, 2002).

For those reasons, in practice it is common to use long measurement records (ranging between 1000 and 2000 times the fundamental period of the structure) that lead to accurate estimates of the modal parameters (Gentile & Saisi, 2013). Alternatively, in this work, an approach which consists in finding *automatically* a free-vibration record segment (time interval with no excitation) within the full measured record of the structural response is proposed. Different methods used in *statistical pattern recognition, computer and robot vision, signal processing* and *system identification* are taken to develop the novel *heuristic* search algorithm. Unlike other proposed methods, this approach besides being output-only has the significant advantage of not imposing conditions on the type of excitation, i. e. the excitation could be non-stationary as in real cases, e.g. on short-span bridges excited by traffic. Classically, the problem of short-time non-stationary stochastic excitation is addressed through input-output methods (Jarczewska, Koszela, Sniady, & Korzec, 2011). Since the parameter identification in the last iteration is performed on the selected free-vibration segment, the proposed algorithm is very accurate and only requires, as input, a relatively short measured record containing it (e.g. 200 times the fundamental period of the structure).

Furthermore, within the *statistical-pattern-recognition damage-detection* paradigm (Farrar et al., 2001; Sohn, 2007; Sohn, Farrar, Hemez, & Czarnecki, 2002), the proposed algorithm can be advantageously used for *data cleansing* (i.e., the process of selectively choosing data to accept for, or reject from, the *feature selection* process), thus mitigating the problems of mass variability and loading interaction (De Roeck et al., 2002; Farrar et al., 2000; Kim et al., 1999). On the other hand, because the need for large amounts of data is drastically reduced, significant implications arise in the design of the SHM hardware (Collins et al., 2014; Dong et al., 2010; Ko & Ni, 2005; Wong, 2004; Wu et al., 2010): less data have to be transmitted; in modem communications, shorter duty-cycles are needed; and, consequently, the power consumption is lower (Collins et al., 2014). The last allows using smaller batteries and solar cells, thus reducing size, weight, cost of remote data-acquisition units and vandalism risk, problems that have been recognized in SHM (Gravengaard, 1986; Housner et al., 1997; Ko & Ni, 2005; Lester, 2001).

Irrespective of implementation details, SHM essentially involves the following stages: 1) *sensor and data acquisition*, 2) *data transfer and communication*, 3) *data analysis and interpretation*, and 4) *data management* (Dong et al., 2010). Thus, the proposed algorithm can be implemented on the first and third stage.

The first option requires a data-acquisition hardware having a relatively powerful processor, but less data have to be transmitted: only the free-vibration record segment or simply the identified modal parameters. In the second option, with less computational demand, the full records have to be transmitted; however, these full records have to be long enough to contain a free-vibration record segment, but not too long to validate the white-noise assumption of the excitation. For this reason, the algorithm is beneficial in both implementation options.

As a counterpart, to ensure that the algorithm finds a free-vibration segment, it is necessary that there is any measuring interval with no excitation. Moreover, the identified system has to be
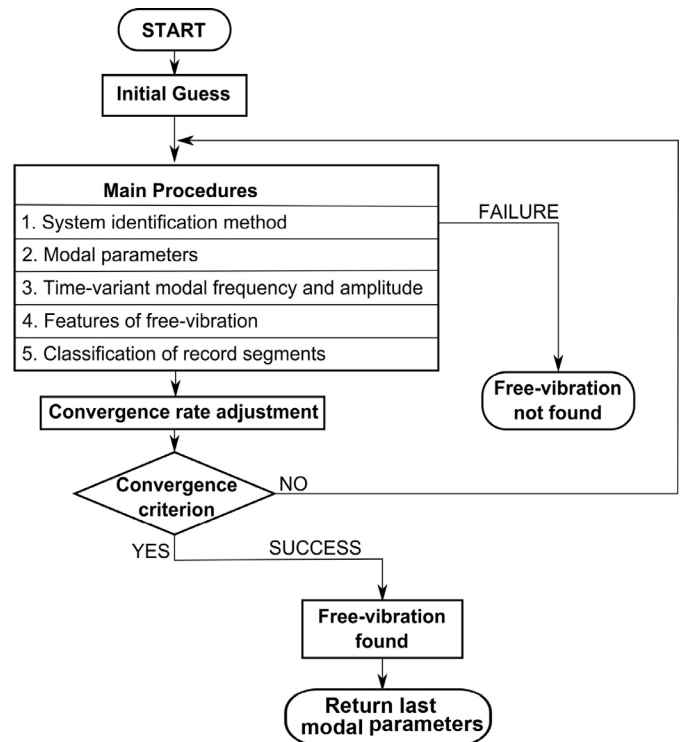

Fig. 1. Flowchart of the heuristic search algorithm.

linear which limits its application e.g. systems under low excitation such as bridges excited by passing cars or moderate wind.

2. Heuristic search algorithm

Heuristic techniques are methods which seek good solutions at a reasonable computational cost without being able to guarantee optimality or even to state how close the optimal solution is (Rayward-Smith, 1996). They are particularly suitable for problems that are hard to solve by classical approaches, as the problem at hand. Thus, in the present work a novel ad-hoc heuristic algorithm is developed to address the problem of finding a free-vibration record segment.

2.1. Overview

As Fig. 1 shows, the algorithm consists of a chain of *main procedures* that aim to search for a free-vibration segment from a measured full record. These procedures are embedded in an iterative scheme which tends to improve the search accuracy of the record segment by *successive approximations*.

The algorithm starts by applying a system identification method to a record segment (procedure 1). This allows finding modal parameters, in procedure 2, that are then used to extract modal responses (by modal filtering) in procedure 3. These modal responses are analysed by means of Hilbert Transform to obtain their respective instantaneous amplitude and frequency. In procedure 4, record samples are classified into free-vibration (decreasing instantaneous amplitude and stable instantaneous frequency) or non-free-vibration (increasing instantaneous amplitude and unstable instantaneous frequency). Finally, in procedure 5, the longest record segment containing samples of free-vibration is identified.

An interesting aspect of the algorithm is that, after each iteration, the accuracy in the search is improved. Thus, when the free-vibration record segment is finally found in the last iteration, the most accurate modal parameter estimates are already available.

A detailed description of each procedure is given in next section.

2.2. Description of each procedure

In this section, the algorithm steps are sequentially described.

2.2.1. Initial guess

The algorithm is firstly fed with a *full record*, which is defined as a sequence of K column vectors $\boldsymbol{y}_k \in \mathbb{R}^{p \times 1}$ ($k = 1, \ldots, K$). Each of these vectors defines one specific instant of time of the K *samples* in which time is discretized and collects the outputs of p vibration sensors.

On the other hand, a *record segment* corresponding to the jth iteration of the procedure is defined as a sequence of column vectors $\boldsymbol{y}_k$ included in the *full record* ranging from a *first* sample index $[k_f]_j \geq 1$ to a *last* sample index $[k_l]_j \leq K$ (i.e., $k = [k_f]_j, \ldots, [k_l]_j$).

The *initial guess* record segment, necessary in the first iteration ($j = 1$), is response-peak based and it is stated by the following sample indexes:

$$[k_f]_1 = \arg \max_{k=1,\ldots,K} \|\boldsymbol{y}_k\|_\infty \tag{1)}$$

$$[k_l]_1 = K, \tag{2}$$

where $\|\cdot\|_\infty$ is the infinity norm. Thus, the initial defined record segment *conservatively* includes at least one true free-vibration record segment, if it is actually present in the full record.

2.2.2. System identification method

The first step of each iteration is the identification of modal parameters, which is performed by the data-driven Stochastic Subspace Identification method (SSI) (Overschee & Moor, 1996; Peeters, 2000). SSI was selected because: (1) it is more advantageous in handling with closely spaced or repeated modes than spectrum-driven methods; and (2) it does not involve non-linear optimization, which makes it fast and, therefore, suitable for iterative schemes (Peeters, 2000). Because of space limitations, SSI is not fully described in this paper; a detailed explanation can be found in Peeters (2000).

The equation of motion of a structure with n_s degrees-of-freedom (DOFs), instrumented with p sensors and subjected to unmeasured stochastic excitation can be recast into the discrete-time state-space form as follows (Peeters, 2000):

$$\boldsymbol{x}_{k+1} = \boldsymbol{A}\boldsymbol{x}_k + \boldsymbol{w}_k \tag{3}$$

$$\boldsymbol{y}_k = \boldsymbol{C}\boldsymbol{x}_k + \boldsymbol{v}_k, \tag{4}$$

where $\boldsymbol{x}_k \in \mathbb{R}^{n \times 1}$ ($n = 2n_s$) is the discrete-time state vector, $\boldsymbol{C} \in \mathbb{R}^{p \times n}$ depends on the sensor locations and gains, $\boldsymbol{w}_k$ and $\boldsymbol{v}_k$ are noise terms, and $\boldsymbol{A} = \exp(\boldsymbol{A_c}\Delta_t) \in \mathbb{R}^{n \times n}$ is the discrete-time system matrix being $\boldsymbol{A_c}$ the continuous-time system matrix and Δ_t^{-1} is the sampling rate.

Matrices $\boldsymbol{A_c}$ and $\boldsymbol{C}$ can be identified with SSI (Overschee & Moor, 1996; Peeters, 2000) by assuming that $\boldsymbol{w}_k$ and $\boldsymbol{v}_k$ are white-noise vectors, which is classically validated by using *full records* $[\boldsymbol{y}_1 \ldots \boldsymbol{y}_K]$ long enough (Gentile & Saisi, 2013). Alternatively, the white-noise assumption is trivially validated if the system is under free-vibration (i.e., $\boldsymbol{w}_k = 0 \ \forall \ k$); since the noise present in the measurements ($\boldsymbol{v}_k$) is commonly assumed as white noise. This alternative is taken as the key idea of the present step, and it is implemented by performing SSI on only a *record segment*, i.e.:

$$[\boldsymbol{A_c}]_j = \text{SSI}_A\left(\left[\boldsymbol{y}_{[k_f]_j} \ldots \boldsymbol{y}_{[k_l]_j}\right], \Delta_t\right) \tag{5}$$

$$[\boldsymbol{C}]_j = \text{SSI}_C\left(\left[\boldsymbol{y}_{[k_f]_j} \ldots \boldsymbol{y}_{[k_l]_j}\right]\right). \tag{6}$$

where the functions SSI_A and SSI_C stand for the "application of SSI".

The system model order is first estimated from the maximal gap between consecutive singular values found by SSI (more sophisticated methods are available in the literature, e.g. Van Der Auweraer & Peeters, 2004). If system poles with no physical meaning appear due to finite record length (Peeters, 2000), they are simply filtered-out by diagonalizing $\boldsymbol{A_c}$ and eliminating the eigenvectors and eigenvalues that are not complex-conjugate pairs with negative real part. Then, the system model order n is the number of complex eigenvectors remaining after filtering. In this work, when $n = 0$ it is said that the SSI has *failed* (see Fig. 1). Note that the identified matrices $\boldsymbol{A_c}$ and $\boldsymbol{C}$ and the identified system model order n could be different for each iteration ($[n]_j = 2[n_s]_j$).

2.2.3. Modal parameters

Once matrices $[\boldsymbol{A_c}]_j$ and $[\boldsymbol{C}]_j$ are available from the record segment $[\boldsymbol{y}_{[k_f]_j} \ldots \boldsymbol{y}_{[k_l]_j}]$, $3[n_s]_j$ modal parameters can be calculated by using the following standard relations:

$$[f_i]_j = \frac{\left|[\lambda_{2i-1}]_j\right|}{2\pi}, \tag{7}$$

$$[\zeta_i]_j = -\frac{\Re\left([\lambda_{2i-1}]_j\right)}{\left|\Im\left([\lambda_{2i-1}]_j\right)\right|}, \tag{8}$$

$$[\phi_i]_j = \left[\phi_{2i-1}^r\right]_j = \left[\phi_{2i}^r\right]_j, \tag{9}$$

in which: f_i, ζ_i and $\phi_i \in \mathbb{R}^{p \times 1}$ are the ith natural frequency, damping ratio and mode shape (projected on sensor locations), respectively ($i = 1, \ldots, [n_s]_j$); ($\lambda_{2i-1}, \lambda_{2i}$) is the ith pair of complex-conjugate eigenvalues of $\boldsymbol{A_c}$; ($\phi_{2i-1}^r, \phi_{2i}^r$) is the ith pair of real mode shapes extracted from the corresponding pair of complex mode shapes ($\phi_{2i-1}^c, \phi_{2i}^c$); and $\Re$ and $\Im$ stand for the real-part and imaginary-part operators. Approximating complex modes with real modes halves the computational cost of subsequent procedures with negligible information loss if damping is assumed proportional or very light (Clough & Penzien, 1995; Wilson, 2002).

The optimum approximations of the n_s real mode shapes ϕ^r can be extracted from the complex mode shapes ϕ^c as follows (Ahmadian, Gladwell, & Ismail, 1995):

$$\phi^r = \Re(\phi^c \exp(j\theta^*)), \tag{10}$$

$$\theta^* = \arg \max_{\theta \in [0, 2\pi)} (\| \Re(\phi^c \exp(j\theta)) \|), \tag{11}$$

where $j = \sqrt{-1}$, $\|\cdot\|$ stands for the Euclidean norm, and a complex mode shape ϕ^c is the projection of an associated complex eigenvector of $\boldsymbol{A_c}$ on the sensor locations through $\boldsymbol{C}$ (Peeters, 2000). That is to say that the real mode shape most correlated with a complex mode shape is the real part of the same complex mode shape rotated such that its real part is maximized.

Modal parameters $[f_i]_j$, $[\zeta_i]_j$, and $[\phi_i]_j$ are calculated in every iteration, until the best version is reached when the algorithm converges.

2.2.4. Modal frequency and amplitude as functions of time

In order to select a free-vibration record segment, it is proposed to analyse the behaviour of the instantaneous-frequency and -amplitude (positive envelope), over time, of each Modal Response (MR) (Wilson, 2002). These MRs can be obtained by filtering the output record $\boldsymbol{y}_k$ using the mode shapes $[\phi_i]_j$ that are already available from Eq. (9), i.e. by using Modal Filters (MFs) (Freudinger, 1991; Preumont, 2011; Tondreau & Deraemaeker, 2013). In its more simple form, a MF is a linear combiner defined as:

$$[g_{ik}]_j = [\boldsymbol{\alpha}_i]_j^\mathsf{T} \boldsymbol{y}_k \tag{12}$$

where $[\boldsymbol{\alpha}_i]_j^T \in \mathbb{R}^{1 \times p}$ is the transpose of the column vector containing the ith reciprocal mode shape $[\boldsymbol{\alpha}_i]_j$ and $[g_{ik}]_j \in \mathbb{R}$ is the kth sample of the ith MR (recall $\boldsymbol{y}_k \in \mathbb{R}^{p \times 1}$). Assuming $n_s < p$, the matrix containing the reciprocal mode shapes can be estimated through the More–Penrose pseudo-inverse of a $(p \times n_s)$ matrix containing the mode shapes $[\phi_i]_j$ (more sophisticated methods are also available, e.g. Freudinger, 1991).

Noteworthy is that the accuracy of a MF only depends on the mode shapes. Then, if their accuracies improve over iterations, accuracy of the obtained MR $[g_{ik}]_j$ will also improve over them.

Instantaneous-frequency and -amplitude can now be calculated since MRs admit *well-behaved* Hilbert Transforms, at least during the free-vibration (Varadarajan & Nagarajaiah, 2004; Yang, Lei, Pan, & Huang, 2003a). Denoting the Hilbert Transform of the signal g_{ik} as $\tilde{g}_{ik} \in \mathbb{R}$, its discrete-time analytic signal $h_{ik} \in \mathbb{C}$ can be efficiently calculated by means of the Fast Fourier Transform (Marple, 1999) and decomposed as follows (Yang et al., 2003a, b):

$$h_{ik} = g_{ik} + \mathrm{j}\tilde{g}_{ik} = A_{ik} \exp(\mathrm{j}\beta_{ik}). \tag{13}$$

If $\tilde{g}_{ik}$ is well-behaved, $[A_{ik}]_j$ is the instantaneous amplitude of the ith MR, at the kth sample, for the jth iteration; and, since β_{ik} is the instantaneous phase, the corresponding instantaneous frequency is calculated as:

$$[f_{ik}]_j = \frac{[\beta_{ik}]_j - [\beta_{i(k-1)}]_j}{2\pi \Delta_t}. \tag{14}$$

2.2.5. Features characterizing free-vibration samples

Since free-vibration response of a MDOF linear system can be characterized by monotonically decreasing amplitude and constant frequency in all its MRs, the following two features are selected to characterize the *samples* of each MR: (1) the change of the instantaneous amplitude ($[\delta A_{ik}]_j$) and (2) the change of the instantaneous frequency ($[\delta f_{ik}]_j$), which are calculated as:

$$[\delta A_{ik}]_j = \begin{cases} 0, & [A_{ik}]_j - [A_{i(k-1)}]_j < 0 \\ \frac{[A_{ik}]_j - [A_{i(k-1)}]_j}{\Delta_t}, & [A_{ik}]_j - [A_{i(k-1)}]_j \geq 0 \end{cases}, \tag{15}$$

$$[\delta f_{ik}]_j = \frac{[f_{ik}]_j - [f_{i(k-1)}]_j}{\Delta_t}. \tag{16}$$

It is worth noting that Eq. (15) considers, in the same way, all *samples* whose instantaneous amplitude is decreasing; irrespective of the decay rate. Instead, the *samples* whose instantaneous amplitude is increasing can be *penalized* according to their growth rates. For its part, Eq. (16) allows *penalizing* the variation of instantaneous frequency according to the change size, regardless of its sign.

At each iteration, these features are collected in a feature vector $[\boldsymbol{\delta}_k]_j$ that fully characterizes the kth sample, i.e.:

$$[\boldsymbol{\delta}_k]_j = \begin{pmatrix} [\delta A_{1k}]_j \\ [\delta f_{1k}]_j \\ \vdots \\ [\delta A_{ik}]_j \\ [\delta f_{ik}]_j \\ \vdots \\ [\delta A_{n_s k}]_j \\ [\delta f_{n_s k}]_j \end{pmatrix} \in \mathbb{R}^{2[n_s]_j \times 1}. \tag{17}$$

At this point, a feature vector that characterizes an "ideal" sample of free-vibration can be simply defined as $[\boldsymbol{\delta}*]_j = 0 \in \mathbb{R}^{2[n_s]_j \times 1}$; i.e., each of the $[n_s]_j$ MRs has constant instantaneous frequency and decreasing instantaneous amplitude.

2.2.6. Classification of record segments

Deterministically, it could be stated that free-vibration occurs at the sample k if $[\boldsymbol{\delta}_k]_j = [\boldsymbol{\delta}*]_j$. However, this would lead to erroneous decisions since approximations can be imprecise in the first iterations in addition to the noise always present. Instead, the Squared Mahalanobis Distance (SMD) (Dervilis, Worden, & Cross, 2015; Jin & Chow, 2013; Nguyen, Chan, Thambiratnam, & King, 2015; Tondreau & Deraemaeker, 2013; Webb & Copsey, 2011) between $[\boldsymbol{\delta}_k]_j$ and $[\boldsymbol{\delta}*]_j$ can be used as a more robust indicator. The SMD has the following benefits: (1) it is dimensionless and scale-invariant, (2) it takes into account the *precision* of the vectors through covariance matrix and (3) it homogenises variables of different nature. The SMD at the kth sample, for the jth iteration, between the vectors $[\boldsymbol{\delta}_k]_j$ and $[\boldsymbol{\delta}*]_j$ is calculated as follows:

$$\left[D_k^2\right]_j = \left([\boldsymbol{\delta}_k]_j - [\boldsymbol{\delta}*]_j\right)^T [\boldsymbol{\Sigma}]_j^{-1} \left([\boldsymbol{\delta}_k]_j - [\boldsymbol{\delta}*]_j\right), \tag{18}$$

where $[\boldsymbol{\Sigma}]_j^{-1} \in \mathbb{R}^{2[n_s]_j \times 2[n_s]_j}$ is the precision matrix, which is calculated as the inverse of the covariance matrix of $[[\boldsymbol{\delta}_1]_j \ldots [\boldsymbol{\delta}_K]_j] \in \mathbb{R}^{2[n_s]_j \times K}$.

Assuming a Gaussian distribution for the K vectors $[\boldsymbol{\delta}_k]_j$, the equation $[D_k^2]_j = 1$ defines a hyper-ellipsoid, centred around $[\boldsymbol{\delta}*]_j$, which is updated in each iteration and divides the space of vectors $[\boldsymbol{\delta}_k]_j$ into two groups (inside and outside the hyper-ellipsoid) with the same number of vectors. Then, each record *sample* can be classified into "free-vibration" or "non-free-vibration" through the following *thresholding classification* (Haralick & Shapiro, 1992) function:

$$[\hat{D}_k^2]_j = \begin{cases} 1, & [D_k^2]_j < 1, \text{ "free-vibration"} \\ 0, & [D_k^2]_j \geq 1, \text{ "non-free-vibration"} \end{cases} \tag{19}$$

Thus, the proposed heuristic approach used in selecting a free-vibration record *segment*, from the classified free-vibration record *samples*, is explained as follows. The sequence of the numbers $[\hat{D}_k^2]_j$ can be considered as a one-dimensional black-and-white image. Then, a labelling function taken from *computer and robot vision* can be used to efficiently label its connected components with consecutive natural numbers $[L_k]_j$ contained in the vector $[\boldsymbol{L}]_j \in \mathbb{R}^{1 \times K}$ (0 represents image background) (Haralick & Shapiro, 1992). Finally, the label of the longest free-vibration record segment is the statistical mode of that vector, i.e. $\mathrm{Mo}([\boldsymbol{L}]_j)$. On this basis, *preliminary* sample indices defining the next free-vibration record segment are calculated by the following expressions:

$$[k_f^*]_{j+1} = \min_{\text{subject to } \mathrm{Mo}([\boldsymbol{L}]_j) = [L_k]_j} \left([k_f]_j \quad \ldots \quad k \quad \ldots \quad [k_l]_j \right), \tag{20}$$

$$[k_l^*]_{j+1} = \max_{\text{subject to } \mathrm{Mo}([\boldsymbol{L}]_j) = [L_k]_j} \left([k_f]_j \quad \ldots \quad k \quad \ldots \quad [k_l]_j \right). \tag{21}$$

As an illustrative example, if $K = 10$, $[k_f]_j = 2$, $[k_l]_j = 10$, and $[\hat{D}_k^2]_j = 0, 1, 0, 1, 1, 1, 0, 0, 1, 1$; the labelling function returns $[\boldsymbol{L}]_j = [0\ 1\ 0\ 2\ 2\ 2\ 0\ 0\ 3\ 3]$; the label of the longest free-vibration record segment is $\mathrm{Mo}([\boldsymbol{L}]_j) = 2$; and, due to Eqs. (20) and (21), $[k_f^*]_{j+1} = 4$ and $[k_l^*]_{j+1} = 6$.

This procedure returns the longest free-vibration record segment, contained in the current record segment, in which all its samples verify $[D_k^2]_j < 1$. Two facts that provide robustness against uncertainties to the algorithm are highlighted: (1) all the samples that randomly verify $[D_k^2]_j < 1$, but do not belong to the longest free-vibration record segment, are automatically discarded; and (2)
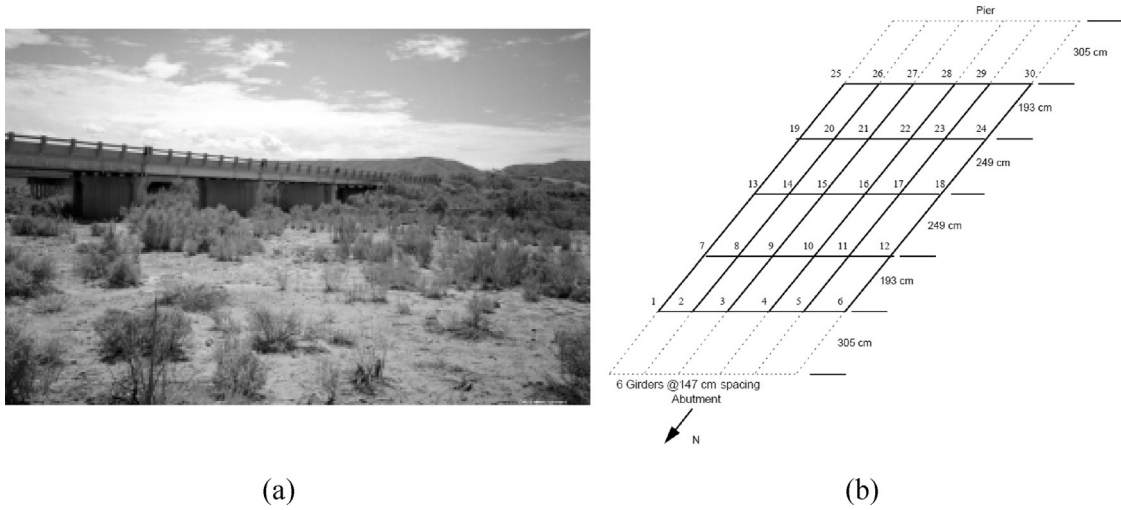
Fig. 2. Alamosa Canyon Bridge: (a) general view and (b) location of the 30 accelerometers on the northernmost span (with permission from Farrar et al., 2000).

if free-vibration is not present, the algorithm returns a record segment that is too short and consequently SSI *fails* in the next iteration (see Fig. 1).

2.2.7. Convergence rate adjustment

Starting from the *current indices* $[k_f]_j$ and $[k_l]_j$, from Eqs. (20) and (21), *preliminary next indices* $[k_f^*]_{j+1}$ and $[k_l^*]_{j+1}$ are obtained. These are now used to generate the *next indices* $[k_f]_{j+1}$ and $[k_l]_{j+1}$ that determine a new more-accurate free-vibration record segment that is contained in the current. This requires that the record segment determined in the iteration j includes, at least, one true free-vibration record segment. The proposed *initial guess* ensures that the requirement is met for $j = 1$. For the subsequent iterations, the following *convergence rate adjustment* aims to meet the requirement by making the convergence more gradual.

A *convergence rate adjustment* is introduced to handle the trade-off between accuracy/robustness and speed. The indices that define the record segment for the next iteration are calculated as the following weighted averages between the *current indices* ($[k_f]_j$, $[k_l]_j$) and the *preliminary next indices* ($[k_f^*]_{j+1}$, $[k_l^*]_{j+1}$):

$$\left[k_f\right]_{j+1} = (1 - r)\left[k_f\right]_j + r\left[k_f^*\right]_{j+1}, \tag{22}$$

$$[k_l]_{j+1} = (1 - r)[k_l]_j + r\left[k_l^*\right]_{j+1}, \tag{23}$$

where $0 < r \leq 1$ is a *tuning parameter* and $\lfloor \cdot \rfloor$ is the "round down" operator (necessary since $k \in \mathbb{N}$). Note that lower values of r lead to slower and smother convergence, avoiding erroneous and/or periodic solutions. Some experience using this algorithm has shown that $r = 0.5$ is a good choice when one or two true free-vibration record segments are present in the full record.

Thus, the indices $[k_f]_{j+1}$ and $[k_l]_{j+1}$ are ready to be used in the next iteration, restarting from Eq. (5); unless one of the following stopping criteria is met.

2.2.8. Stopping criteria

The algorithm can stop, in the *J*th iteration, in two cases, reporting: *success* (the best free-vibration record was found) when $[k_f]_{J+1} = [k_f]_J$ and $[k_l]_{J+1} = [k_l]_J$ or *failure* when $[n]_{J+1} = 0$. Note that neither tolerance nor maximum number of iterations is needed since algorithm stopping is guaranteed.

When the algorithm stops reporting *success*, the identified modal parameters are already available from Eqs. (7)–(9). Besides, the free-vibration record segment is also available for further analysis (e.g. as in Curadelli, Riera, Ambrosini, & Amani, 2008 or in

Cavaleri & Papia, 2014). On the contrary, when the algorithm stops reporting *failure*, the full record can be classified as having no free-vibration or, eventually, discarded to avoid future erroneous estimations.

3. Application to bridge SHM

The algorithm developed in Section 2 can be used for output-only system identification in any application in which the ambient- or operational-loading is composed of short or long impulses (Clough & Penzien, 1995). In the present section, an example on a particular case of bridge SHM illustrates how the algorithm works and demonstrates its benefits.

3.1. Experimental example

In this section, the identification of modal parameters is carry out by the proposed algorithm by using ambient acceleration records taken by the staff of LANL (Farrar et al., 2000) on the Alamosa Canyon Bridge. The dataset is currently available at the website of LANL (Farrar, Cornwell, Doebling, & Prime, 2015) under the name "Ambient Test".

3.1.1. Description of the instrumented structure

Fig. 2(a) shows the Alamosa Canyon Bridge, which has seven independent spans with a common pier between successive spans. The northernmost span of the bridge was instrumented with a grid of 30 accelerometers as shown in Fig. 2(b). A full description of the setup can be found in Farrar et al. (2000).

In the study, eleven ambient vibration records caused by the passage of a Ford Taurus sedan over the bridge were used. Each full record consists of 30 simultaneous acceleration records lasting 16 s each ($K = 2048, \cdot \Delta_t = 0.0078$ s). A basic data-cleansing process was applied to the records before feeding the algorithm: the mean values were removed and some channels containing extremely anomalous readings were discarded.

Table 1
Baseline modal parameters and 95% confidence intervals (CIs).

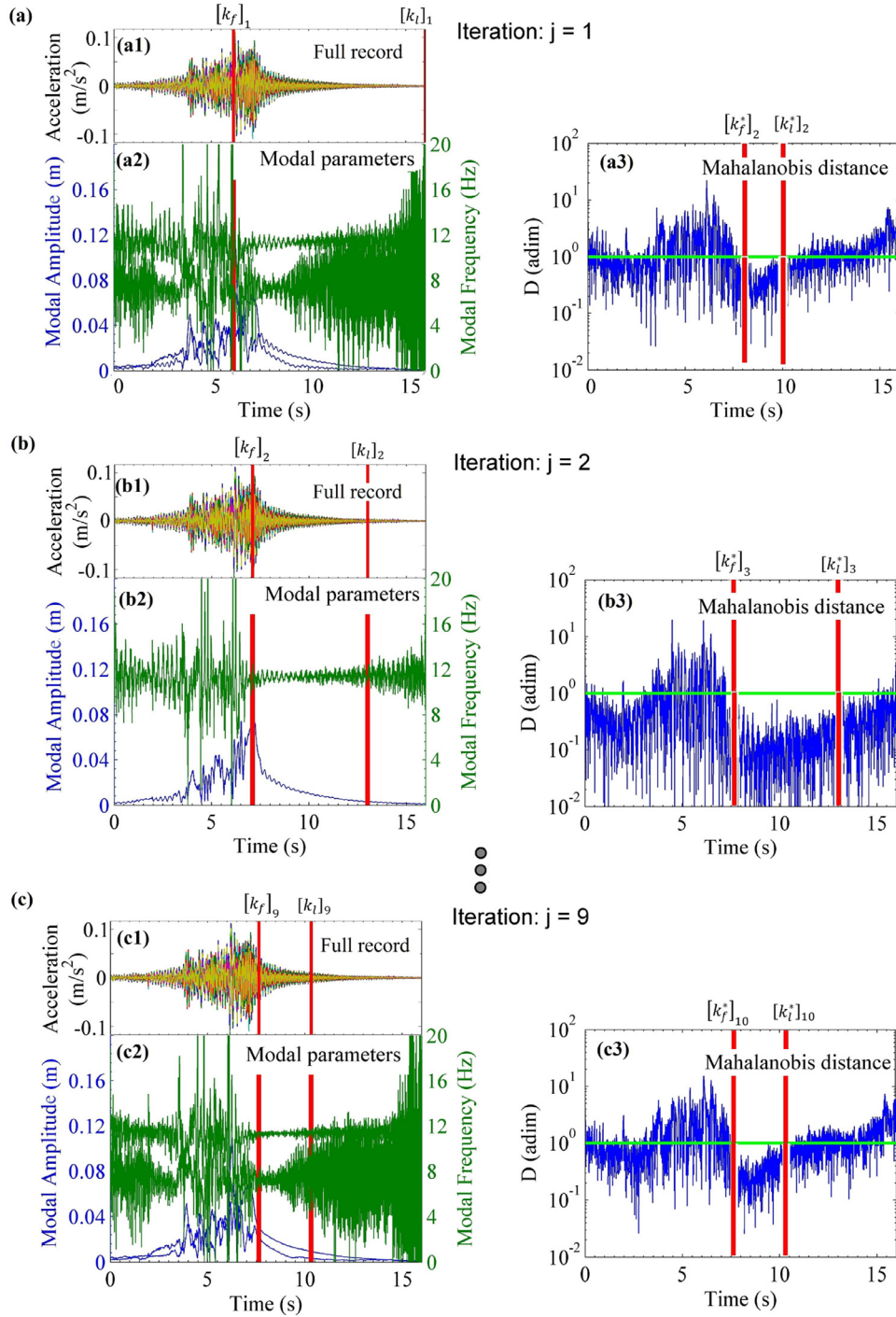| Mode number	Mean modal frequency f_i^*	Mean modal damping ratio ζ_i^*
1	7.32 Hz ($\pm$0.007 Hz)	2.2% ($\pm$0.083%)
2	8.08 Hz ($\pm$0.033 Hz)	1.6% ($\pm$0.250%)
3	11.5 Hz ($\pm$0.018 Hz)	1.3% ($\pm$0.086%)

Fig. 3. Intermediate results for the case 'success (intuitive)'.

3.1.2. Baseline data

Since there is no information concerning the excitation time histories, identified modal parameters taken from Farrar et al. (2000) were used as reliable baseline data to assess the performance of algorithm (see Table 1). The identified parameters were estimated with a Monte Carlo analysis of averaged Frequency Response Functions from 330 measurements (at each acceleration channel) recorded over a 24 h time period from July to August 1996, by using as excitation roving hammer impacts while the bridge was unloaded.

In this particular case where baseline data are available, the algorithm convergence is demonstrated from the two modal-parameter estimation errors calculated for every iteration as follows:

$$[\text{Error}(f_i)]_j = \frac{[f_i]_j - f_i^*}{f_i^*}, \ i = 1, \ldots, [n_s]_j \tag{24}$$

$$[\text{Error}(\zeta_i)]_j = \frac{[\zeta_i]_j - \zeta_i^*}{\zeta_i^*}, \ i = 1, \ldots, [n_s]_j \tag{25}$$

Then, from modal-parameter estimation errors at last iteration $(j = J)$, the algorithm performance is assessed.

3.2. Results and discussion

The algorithm was fed with each of the eleven available full records, using $r = 0.5$ in Eqs. (22) and (23). Because of space limitations, only two *successful* cases are thoroughly reported: one whose results are *intuitive* and the other *non-intuitive*. These representative scenarios demonstrate that the developed algorithm performs as well as a human *expert* in evident cases and can also cope with cases that are misleading for human *experts*.

To assess the benefits inherent to the searching algorithm proposed in this work, two alternatives commonly used were outlined. The first basic alternative consisted of the application of SSI on the full record but, the results obtained were very inaccurate and were discarded. The second alternative, with easy implementation, consisted in using SSI simply with the response-peak based *initial guess*. The results were uneven depending on the existence of free-vibration segments. Thus, the performance of the proposed algorithm was quantified in terms of the errors obtained at the last iteration $[\text{Error}(f_i)]_J$, $\cdot[\text{Error}(\zeta_i)]_j$. with regard to those obtained by the second alternative, $[\text{Error}(f_i)]_1$, $\cdot[\text{Error}(\zeta_i)]_1$.

3.2.1. Intuitive case

This case correspond to the file named as "sp1_am05" in Farrar et al. (2000). Fig. 3(a,b,c) shows the evolution of the main variables for the first ($j = 1$), second ($j = 2$) and last iteration ($j = J = 9$). Full record $\mathbf{y}_k$ in Fig. 3(a1,b1,c1); instantaneous amplitude A_{ik} and instantaneous frequency f_{ik} of each MR in Fig. 3(a2,b2,c2); and Mahalanobis Distance D_k in Fig. 3(a3,b3,c3). Besides, red vertical lines represent indices $[k_f]_j$, $[k_l]_j$, $[k_f^*]_{j+1}$ and $[k_l^*]_{j+1}$.

The present case results *intuitive* in the sense that a human *expert* that thoroughly inspects Fig. 3(a1) could *rightly* suggest that free-vibration occurs from $t = 7.3$ s and noise dominates the response after $t = 13$ s approximately.

Because the instantaneous frequencies are steady and instantaneous amplitudes are decreasing during the time interval, the location of the free-vibration record segment can be easily identified from Fig. 3(a2, b2, c2). Clearly, the noise components on these variables are vanishing as iterations proceed. This demonstrates the assumption that the accuracy of modal identification improves with iterations.

It is worth noting that despite the differences in feature distributions, because of the SMD robustness, the algorithm finds a free-vibration segment in all iterations (see Fig. 3(a3, b3, c3)).

The vertical lines in Fig. 3(c2, c3) show that the identified free-vibration record segment is the same for the last two iterations (i.e., $[k_f]_9 = [k_f^*]_{10} = [k_f]_{10}$ and $[k_l]_9 = [k_l^*]_{10} = [k_l]_{10}$). This means that the algorithm converges and, therefore, reports *success* and returns the identified modal-parameters.

Fig. 4 shows the errors over iterations. The *initial guess* provides a significant but still insufficient accuracy (Error(f_1) = 4%, Error(f_2) = 10%, Error(ζ_1) = 15%, Error(ζ_2) = 700%). These errors can be due to the fact that the long-lasting loading, which is evident since the response peak occurs during the forced phase (see Fig. 3(c1, c2) at $t = 6$ s), which hampers the identification process.

Fig. 4 demonstrates that, in an average sense, the accuracy of modal parameter estimation improves over iterations. As expected, damping dispersion is greater (see Table 1 and Curadelli et al., 2008; Peeters, 2000).

In the last iteration (i.e. $j = J = 9$), the algorithm returns modal parameters very accurately (Error(f_1) = 0.9%, Error(f_3) = 1.7%, Error(ζ_1) = 12%, Error(ζ_3) = 50%). In general terms, the algorithm provides estimates of the modal parameters that are five times more accurate than those obtained using a typical SSI process with a response-peak based *initial guess*. It is worth noting that the mode that was not identified (mode number 2 in Table 1) is the one having the largest CIs (see Table 1).
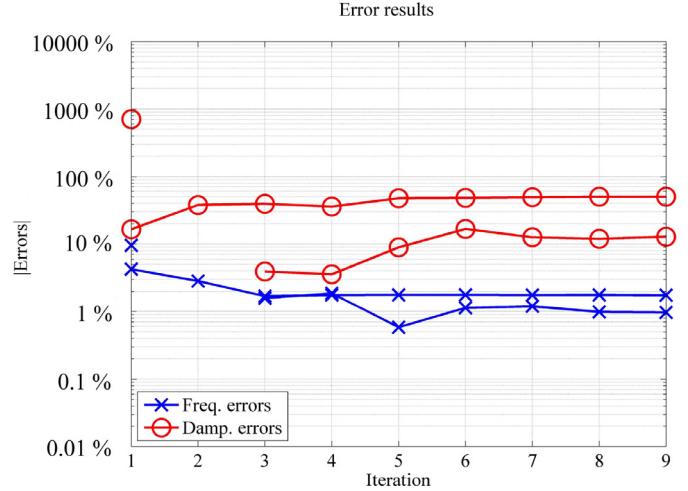

Fig. 4. Errors for the case: 'success (intuitive)'.

3.2.2. Non-intuitive case

This example correspond to the file named as 'sp1_am07' in Farrar et al. (2000). Fig. 5(a, b, c) shows, respectively for $j = 1$, 2, J, the evolution of the main variables of the algorithm. The result in this case is *non-intuitive* in the sense that the best free-vibration record segment *seems to be located* in the time interval 5.5 s < t < 12 s, which is indeed false.

Fig. 5(a2) shows that, with the *initial guess*, only one mode is identified ($[n_s]_1 = 1$). It also shows that the instantaneous amplitude and instantaneous frequency of that mode are very noisy in the time interval in which the free-vibration record segment *seems to be located*. Interestingly, in the time interval 12 s < t < 15 s, the instantaneous amplitude is not increasing and the instantaneous frequency is more stable. Then, feature vectors $[\boldsymbol{\delta}_k]_1$ having values of k belonging to that time interval are inside the hyper-ellipse defined by $[D_k^2]_j = 1$, which is confirmed in Fig. 5(a3).

Fig. 5(b2) shows that, for the second iteration, the selected record segment tends to the time interval 12 s < t < 15 s; though the record segment starts conservatively at 8.8 s, thanks to the *convergence rate adjustment*. Fig. 5(b2) shows an evident free-vibration record segment in the time interval 8.8 s < t < 10.4 s. However, this record segment is not the longest with similar characteristics, and therefore, it is discarded by the algorithm on the next iteration (see Fig. 5(b3)) reducing the possibility of undesired *failure*.

Fig. 5(c2, c3) shows that the record segment *successfully* converges (in the iteration $j = J = 12$) to a solution which is *non-intuitive*. Fig. 5(c2) shows that, in the found record segment, the instantaneous amplitude is not decreasing; however, it is not increasing either and the noise is almost absent. The instantaneous frequency, for its part, looks quite stable as compared to other time intervals. It is highly likely that, in that time interval, only one mode contributes significantly to the response. With these evidences, it is difficult to know the type of excitation that the structure was subjected to; in either case, however, the record segment found by the algorithm was suitable to accurately estimate the modal parameters as demonstrated by the following error results.

Fig. 6 shows that errors obtained by using the *initial guess* are inadmissible for damage detection (Error(f_1) = 8.1%, Error(ζ_1) = 130%). The algorithm, after successive iterations, reduces the frequency error by ten times (Error(f_1) = 0.7%) and the damping ratio error by 40% (Error(ζ_1) = 77%). It is worth recalling that, when using SSI, damping estimation errors can easily get as high as 100% when the stationary condition is not satisfied (Ceravolo, 2004). Second and third Modes could not be identified, given they have the largest CIs (see Table 1).
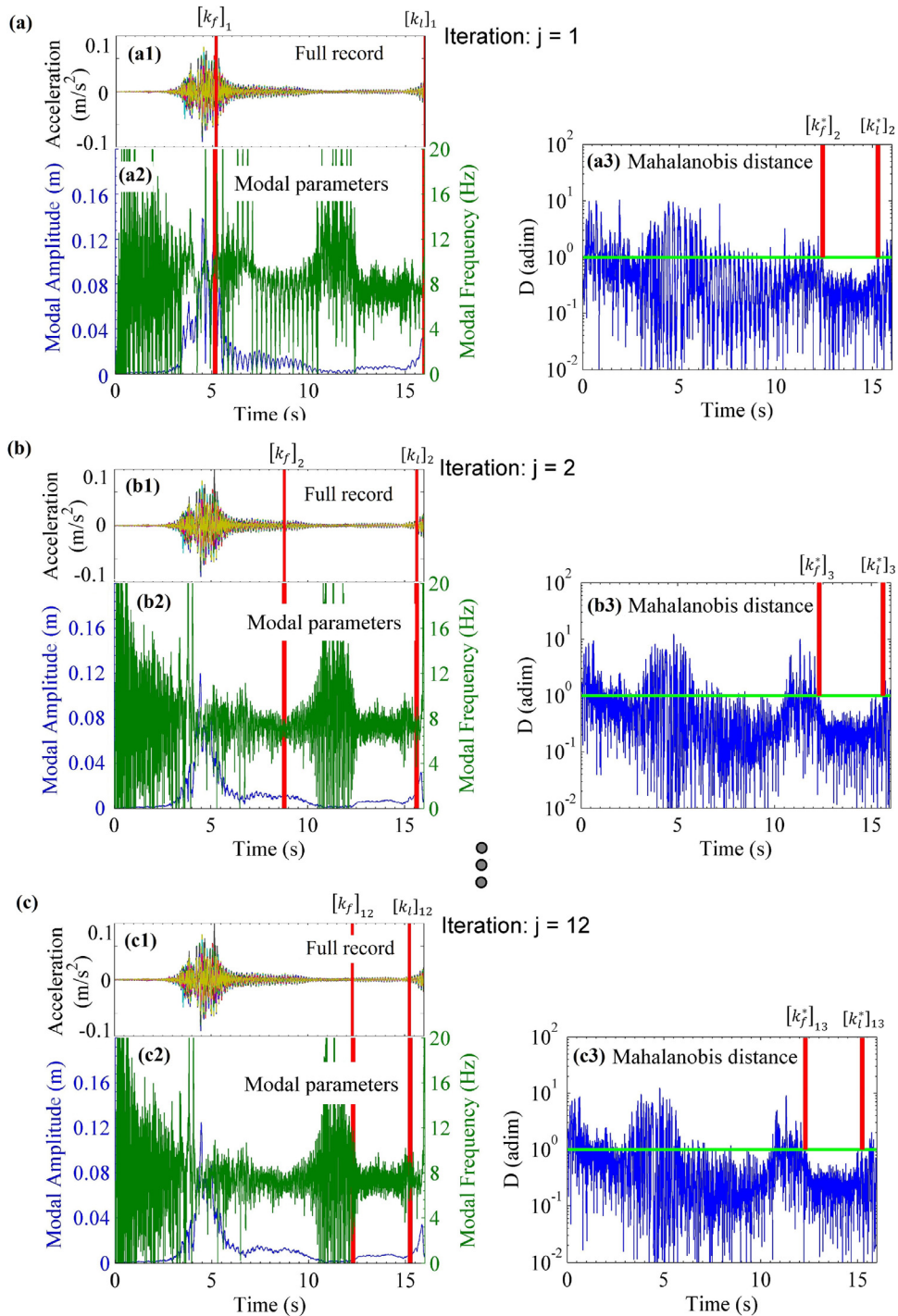
Fig. 5. Intermediate results for the case 'success (non-intuitive)'.

The error peak that Fig. 6 shows around iteration 7 is explained as follows. The indices $[k_f]_7$ and $[k_l]_7$ correspond to the time interval $12\,\mathrm{s} < t < 15.2\,\mathrm{s}$, which excludes one of the free-vibration record segments (see decreasing amplitude and stable frequency in the time interval $8.8\,\mathrm{s} < t < 10.4\,\mathrm{s}$ in Fig. 5(c2)) but includes the forced phase occurring in the time interval $12\,\mathrm{s} < t < 12.5\,\mathrm{s}$ (distinguishable by increasing amplitude). In the latter time interval, the frequency content and non-stationarity of excitation cause the large errors in natural frequency and damping, respectively. This example demonstrates that if more than one true free-vibration record segment is present in the full record, the errors of modal parameter estimation can be decreasing only in an av-

erage sense, even when the accuracy of the free-vibration record segment is strictly increasing. Note that, though the algorithm does not return the optimal modal parameters (e.g., stopping at $j = 5$), it returns very good approximations, as it is usually expected from heuristic methods.

4. Conclusions

For the problem of output-only system identification under non-white-noise random excitation, an algorithm based on the heuristic search of free-vibration record segments has been developed and tested with experimental data. The algorithm is fully
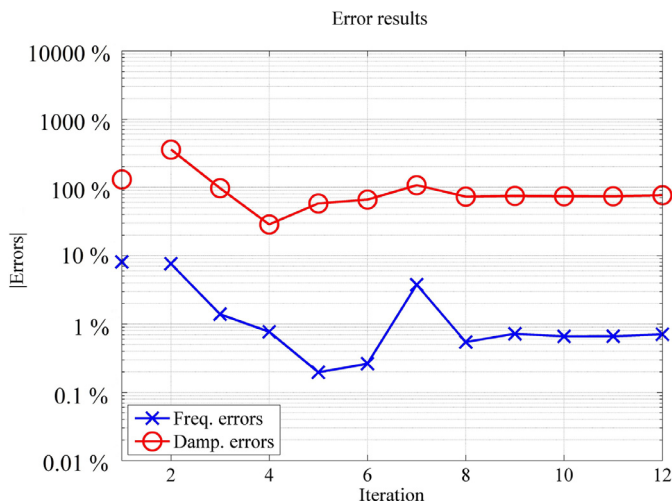
Error results

Fig. 6. Estimation errors for the case: 'success (non-intuitive)'.

automatic and it only has the convergence rate as tuning parameter. Besides, it is intrinsically prevented from false parameter identification if, for example, there is no clearly a free-vibration segment by the presence of noise.

Through an experimental example, it was demonstrated that the proposed method allows estimating modal parameters with up to ten times more accuracy than that obtained by applying the same system identification method to a record segment starting at the response peak. Specifically, all of the *successful* cases displayed frequency errors under 2%.

As compared to the classical approach in which full long records are used, the advantages in the SHM hardware are evident.

Acknowledgements

References

Ahmadian, H., Gladwell, G. M. L., & Ismail, F. (1995). Extracting real modes from complex measured modes. In *Proceedings of spie - the international society for optical engineering* (pp. 507–510).

Cavaleri, L., & Papia, M. (2014). An output-only stochastic parametric approach for the identification of linear and nonlinear structures under random base excitations: Advances and comparisons. *Probabilistic Engineering Mechanics, 35*, 11–21. doi:10.1016/j.probengmech.2013.10.010.

Ceravolo, R. (2004). Use of instantaneous estimators for the evaluation of structural damping. *Journal of Sound and Vibration, 274*, 385–401. doi:10.1016/j.jsv.2003.05.025.

Chen, B., & Zang, C. (2011). A hybrid immune model for unsupervised structural damage pattern recognition. *Expert Systems and Application, 38*, 1650–1658. doi:10.1016/j.eswa.2010.07.087.

Clough, R. W., & Penzien, J. (1995). *Dynamics of structures* (3rd ed.). Berkeley, CA 94704 USA: Computers & Structures, Inc..

Collins, J., Mullins, G., Lewis, C., & Winters, D. (2014). *State of the practice and art for structural health monitoring of bridge substructures.*

Curadelli, R. O., Riera, J. D., Ambrosini, D., & Amani, M. G. (2008). Damage detection by means of structural damping identification. *Engineering Structures, 30*, 3497–3504. doi:10.1016/j.engstruct.2008.05.024.

De Roeck, G., Maeck, J., Michielsen, T., & Seynaeve, E. (2002). Traffic-induced shifts in modal properties of bridges. *Proc. IMAC 20, 4753*, 630–636.

Dervilis, N., Worden, K., & Cross, E. J. (2015). On robust regression analysis as a means of exploring environmental and operational conditions for SHM data. Journal of Sound and Vib*ration. doi:10.1016/j.jsv.2015.02.039.

Dong, Y., Song, R., & Liu, H. (2010). *Bridges structural health monitoring and deterioration detection - Synthesis of knowledge and technology*. Alaska: John Wiley & Sons, Inc.

Ewins, D. (1984). *Modal testing: Theory and practice* New York, Brisbane, Chichester, Toronto, Singapore.

Farrar, C. R., Cornwell, P. J., Doebling, S. W., & Prime, M. B. (2000). *Structural health monitoring studies of the alamosa canyon and I-40 bridges* Los Alamos, New Mexico.

Farrar, C. R., Cornwell, P. J., Doebling, S. W., & Prime, M. B. (2015). LANL - engineering institute [www document]. *SHM Data Sets and Software*. http://www.lanl.gov/projects/national-security-education-center/engineering/software/shm-data-sets-and-software.php.

Farrar, C. R., Doebling, S. W., & Nix, D. A. (2001). Vibration-based structural damage identification. *Philosophical Transactions of the Royal Society A Mathematical, Physical and Engineering Science, 359*, 131–149. doi:10.1098/rsta.2000.0717.

Freudinger, L. C. (1991). *Analysis of structural response data using discrete modal filters* California.

Gentile, C., & Saisi, A. (2013). Operational modal testing of historic structures at different levels of excitation. *Construction and Building Materials, 48*, 1273–1285. doi:10.1016/j.conbuildmat.2013.01.013.

Gravengaard, G. B. (1986). Use of computers in the field. *Ground Water Monitoring & Remediation, 6*, 126–128. doi:10.1111/j.1745-6592.1986.tb01253.x.

Haralick, R. M., & Shapiro, L. G. (1992). *Computer and robot vision*: volume 1 (1st ed.). Massachusetts: Addison-Wesley Publishing Company.

Housner, G. W., Bergman, L. A., Caughey, T. K., Chassiakos, A. G., Claus, R. O., Masri, S. F., et al. (1997). Structural control: Past, present, and future. *Journal of Engineering Mechanics, 123*, 897–971.

Ibrahim, S. R. (1977). Random decrement technique for modal identification of structures. *Journal of Spacecraft and Rockets, 14*, 696–700. doi:10.2514/3.57251.

Jarczewska, K., Koszela, P., Sniady, P., & Korzec, A. (2011). Identification of the structure parameters using short-time non-stationary stochastic excitation. *Journal of Sound and Vibration, 330*, 3352–3367. doi:10.1016/j.jsv.2011.02.019.

Jin, X., & Chow, T. W. S. (2013). Anomaly detection of cooling fan and fault classification of induction motor using Mahalanobis-Taguchi system. *Expert Systems with Applications, 40*, 5787–5795. doi:10.1016/j.eswa.2013.04.024.

Kim, C. Y., Jung, D. S., Kim, N. S., & Yoon, J. G. (1999). Effect of vehicle mass on the measured dynamic characteristics of bridges from traffic-induced vibration test. In *IMAC XIX. Kissimmee, FL* (pp. 1106–1111).

Ko, J. M., & Ni, Y. Q. (2005). Technology developments in structural health monitoring of large-scale bridges. *Engineering Structures, 27*, 1715–1725. doi:10.1016/j.engstruct.2005.02.021.

Kramer, C., De Smet, C. A. M., & Peeters, B. (1999). Comparison of ambient and forced vibration testing of civil engineering structures. In *17th Int. Modal Anal. Conf.* (pp. 1030–1034).

Lester, A. (2001). Crime Reduction through Product Design. *Trends & Issues in Crime and Criminal. Justice.*

Marple, S. L. (1999). Computing the discrete-time «analytic» signal via FFT. *2600 IEEE Transaction on Signal Processing, 47*, 2600–2603.

Miguel, L. F. F., Miguel, L. F. F., Kaminski, J., & Riera, J. D. (2012). Damage detection under ambient vibration by harmony search algorithm. *Expert Systems with Applications, 39*, 9704–9714. doi:10.1016/j.eswa.2012.02.147.

Nguyen, T., Chan, T. H. T., Thambiratnam, D. P., & King, L. (2015). Development of a cost-effective and flexible vibration DAQ system for long-term continuous structural health monitoring. *Mechanical Systems and Signal Processing*, 1–12. doi:10.1016/j.ymssp.2015.04.003.

Van Overschee, P., & De Moor, B. (1996). *Subspace identification for linear systems: Theory, implementation, applications.*. Boston/London/Dordrecht: Kluwer Academic Publishers Kluwer Academic Publishers.

Peeters, B. (2000). *System identification and damage detection in civil engineering.* Katholieke Universiteit Leuven.

Preumont, A. (2011). vibration control of active structures: an introduction. *Civil engineering, solid mechanics and its applications* (3rd ed.). NetherlandsDordrecht: Springer. doi:10.1007/978-94-007-2033-6.

Rayward-Smith, V. J. (1996). *Modern heuristic search methods*. United Kingdom: John Wiley & Sons, Ltd.

Salem, H. M., & Helmy, H. M. (2014). Numerical investigation of collapse of the Minnesota I-35 W bridge. *Engineering Structures, 59*, 635–645. doi:10.1016/j.engstruct.2013.11.022.

Sohn, H. (2007). Effects of environmental and operational variability on structural health monitoring. *Philosophical Transactions of the Royal Society A Mathematical, Physical and Engineering Science, 365*, 539–560. doi:10.1098/rsta.2006.1935.

Sohn, H., Farrar, C. R., Hemez, F., & Czarnecki, J. (2002). A review of structural health monitoring literature 1996 – 2001. In *Third world conference on structural control* (pp. 1–7).

Tondreau, G., & Deraemaeker, A. (2013). Local modal filters for automated data-based damage localization using ambient vibrations. *Mechanical Systems and Signal Processing, 39*, 162–180. doi:10.1016/j.ymssp.2013.03.020.

Van Der Auweraer, H. &, & Peeters, B. (2004). Discriminating physical poles from mathematical poles in high order systems: Use and automation of the stabilization diagram. In *Conference record - IEEE Instrumentation and Measurement Technology Conference: 3* (pp. 2193–2198). doi:10.1109/IMTC.2004.1351525.

Varadarajan, N., & Nagarajaiah, S. (2004). Wind response control of building with variable stiffness tuned mass damper using empirical mode decomposition/hilbert transform. *Journal of Engineering Mechanics, 130*, 451. doi:10.1061/(ASCE)0733-9399(2004)130:4(451).

Webb, A. R., & Copsey, K. D. (2011). *Statistical pattern recognition* (3re ed.). United Kingdom: John Wiley & Sons, Ltd.

Wilson, E. L. (2002). *Three-dimensional static and dynamic analysis of structures* (3rd ed.). Berkeley, California: Computers and Structures, Inc..

Wong, K. Y. (2004). Instrumentation and health monitoring of cable-supported bridges. *Structural Control and Health Monitoring, 11*, 91–124. doi:10.1002/stc.33.

Wu, J., Yuan, S., Ji, S., Zhou, G., Wang, Y., & Wang, Z. (2010). Multi-agent system design and evaluation for collaborative wireless sensor network in large structure health monitoring. *Expert Systems with Applications, 37*, 2028–2036. doi:10.1016/j.eswa.2009.06.098.

Yang, J. N., Lei, Y., Pan, S., & Huang, N. (2003a). System identification of linear structures based on Hilbert-Huang spectral analysis. Part 1: Normal modes. *Earthquake Engineering & Structural Dynamics, 32*, 1443–1467. doi:10.1002/eqe.287.

Yang, J. N., Lei, Y., Pan, S., & Huang, N. (2003b). System identification of linear structures based on Hilbert–Huang spectral analysis. *Part 2: Complex modes. Earthquake Engineering & Structural Dynamics, 32*, 1443–1467. doi:10.1002/eqe.287.